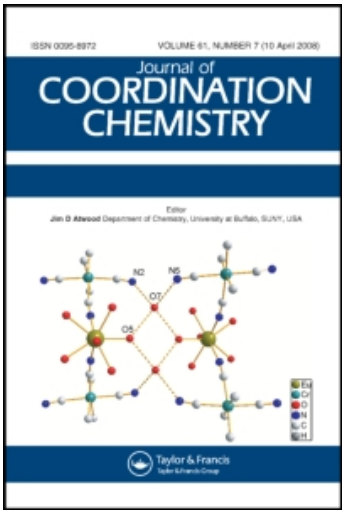

Journal of Coordination Chemistry
Publication details, including instructions for authors and subscription information:
http://www.informaworld.com/smpp/title~content=t713455674

On the way to monodispersed ZnO nanocrystals: structure of a zinc dimer bearing primary amido ligands

Bing Luo[a]; Wayne L. Gladfelter[a]
[a] Department of Chemistry, University of Minnesota, Minneapolis, MN 55455, USA

Online publication date: 17 January 2011

To cite this Article Luo, Bing and Gladfelter, Wayne L.(2011) 'On the way to monodispersed ZnO nanocrystals: structure of a zinc dimer bearing primary amido ligands', Journal of Coordination Chemistry, 64: 1, 82 — 92
To link to this Article: DOI: 10.1080/00958972.2010.543460
URL: http://dx.doi.org/10.1080/00958972.2010.543460

Journal of Coordination Chemistry
Vol. 64, No. 1, 10 January 2011, 82–92

Taylor & Francis
Taylor & Francis Group

On the way to monodispersed ZnO nanocrystals: structure of a zinc dimer bearing primary amido ligands

BING LUO and WAYNE L. GLADFELTER*

Department of Chemistry, University of Minnesota, 207 Pleasant St. SE, Minneapolis, MN 55455, USA

(*Received 7 September 2010; in final form 16 November 2010*)

The two-stage conversion of $[Zn(N^iBu_2)_2]_2$ into nanocrystals of zinc oxide has been studied. The initial reaction of $[Zn(N^iBu_2)_2]_2$ with hexylamine in ether was conducted under nitrogen and required the addition of two hexylamines for each molecule of $[Zn(N^iBu_2)_2]_2$. After 18 h the clear precursor solution contained free diisobutylamine, $[Zn(N^iBu_2)_2]_2$ and an oligomeric zinc species. In the second stage of the reaction, the nitrogen atmosphere was replaced with a flow of moist air. Over a period of 2.5–4 days the water in the atmosphere hydrolyzed the zinc amide bonds, and the CO_2 converted much of the hexylamine into hexylammonium hexylcarbamate, which served as the stabilizing surfactant. Based on powder X-ray diffraction there was a long period during which crystalline ZnO nucleated followed by relatively rapid growth. Replacing hexylamine with the bulky aniline derivative, 2,6-diisopropylaniline, in the first stage of the reaction made it possible to isolate and characterize a new crystalline dinuclear product, $[Zn(NH\text{-}2,6\text{-}^iPr_2C_6H_3)_2]_2(HN^iBu_2)$, bearing two bridging and two terminal primary amido ligands. One of the zincs was tricoordinate, whereas the second zinc was four coordinate as a result of binding a molecule of diisobutylamine.

Keywords: Zinc; Nanocrystals; Amido

1. Introduction

Zinc oxide is a wide bandgap semiconductor used in a variety of areas including catalysis, pigments, and optoelectronics [1]. As with other semiconductor nanoparticles, the properties of ZnO depend on the size when the crystal diameter drops below approximately 6 nm [2, 3]. Methods of preparing monodispersed nanocrystals of ZnO are widely available [4]. In a recent publication [5], we outlined an approach that resulted in gram quantities of nanocrystals stabilized by hexylammonium hexylcarbamate. The reaction occurs in two distinct stages, and in this report we describe the results that help identify some of the chemistry involved in each stage. While we were unable to isolate crystalline intermediates in the actual synthesis, we were able to prepare and characterize a new dinuclear zinc complex with primary amido (RNH^-) ligands that we propose is related to the intermediate formed in the first stage of the conversion.

*Corresponding author. Email: wlg@umn.edu

Journal of Coordination Chemistry
ISSN 0095-8972 print/ISSN 1029-0389 online © 2011 Taylor & Francis
DOI: 10.1080/00958972.2010.543460

2. Experimental

Toluene and hexanes were dried with alumina in an MBraun solvent purification system. Diethyl ether, pentane, benzene-d_6, deuterated chloroform, diisobutylamine (HN^iBu_2), hexylamine ($HexNH_2$), and 2,6-diisopropylaniline were distilled over calcium hydride under nitrogen. Acetone and ethanol were dried over 4A molecular sieves and distilled under N_2. Bis(diisobutylamido) zinc, $[Zn(N^iBu_2)_2]_2$, was prepared as a colorless crystalline solid according to the method described in the literature [6]. The samples were handled using standard air-free techniques. NMR spectra were obtained in C_6D_6 or $CDCl_3$ solutions at room temperature on a Varian INOVA 300 spectrometer. The ^1H NMR spectra were referenced to residual proton at 7.15 ppm in C_6D_6 or 7.27 ppm in $CDCl_3$. The ^{13}C NMR spectra were referenced to the carbon resonance at 128.39 ppm for C_6D_6 or 77.23 ppm for $CDCl_3$. Infrared (IR) spectra of solids (KBr pellets) or liquids (NaCl windows) were recorded on a Nicolet MAGNA-IR 560 spectrometer. Elemental analyses were performed by Desert Analytics, Tucson, AZ. The powder X-ray diffraction (XRD) measurements were conducted on a Bruker-AXS Microdiffractometer equipped with an area detector. A Cu X-ray source operated at 45 kV and 40 mA was used. All data collection used a frame time of 100 s. A standard LaB_6 sample was used to calibrate the instrumental peak broadening. Datascan software was used for XRD data fitting and crystal size calculations. All of the XRD sizes reported here were calculated with the Scherer equation using the 102 reflection.

2.1. *Stage 1: reaction of $[Zn(N^iBu_2)_2]_2$ with two equivalents of hexylamine*

To a solution of $[Zn(N^iBu_2)_2]_2$ (3.00 g, 4.66 mmol) in 60 mL of Et_2O under N_2 at room temperature was added hexylamine (1.23 mL, 9.32 mmol) *via* a syringe. A white precipitate formed immediately, but it dissolved after stirring for 3 h. The solution was stirred for an additional 15 h, followed by the removal of volatiles under prolonged vacuum pumping (8 h). A colorless, viscous liquid (*ca* 3 g) was obtained. IR (NaCl windows, cm^{-1}): 2955 m, 2921 m, 2871 m, 2851 m, 1467 s, 1378 s, 1368 m sh, 1261 m, 1141 w, 1102 s, 1064 s, 1036 s, 1022 s, 993 m sh, 953 w, 923 w, 889 w, 875 w, 805 s, 761 m, 725 m. ^1H and ^{13}C NMR results are given below.

2.2. *Stage 2: addition of water and particle growth*

Using the optimum procedure [5] for making ZnO, 2.46 mL of hexylamine (18.6 mmol), 6.00 g of $[Zn(N^iBu_2)_2]_2$ (9.32 mmol), and 100 mL of Et_2O were added to the flask. After an air flow (relative humidity of $35 \pm 1\%$) was introduced over the solution, a white solid appeared within 1 day. At 83 h, the solution (*ca* 10 mL) became clear. Starting from this point, aliquots of the solution (0.5–1.0 mL) were isolated at 83, 89, 95, 107, 113, and 119 h, and ZnO samples (0.11–0.20 g) were obtained after filtration and evaporation of volatiles. The volatiles were also collected using a liquid N_2 trap and analyzed with NMR spectroscopy. After 119 h, the remaining material (*ca* 0.5 mL) was allowed to dry to form a waxy solid at 133 h (0.23 g). The temperature during synthesis was $20 \pm 1^\circ C$. The ZnO samples were characterized with UV-Vis absorption spectroscopy, XRD, and TEM.

2.3. *Synthesis of [Zn(NH-2,6-^{i}Pr$_2$C$_6$H$_3$)$_2$]$_2$(HN^{i}Bu$_2$)*

The synthesis used standard air-free techniques. To a solution of $[Zn(N^iBu_2)_2]_2$ (3.00 g, 4.66 mmol) in 50 mL of Et_2O at room temperature, 2,6-^{i}Pr$_2$C$_6$H$_3$NH$_2$ (1.76 mL, 9.32 mmol) was added. A pale yellow solution formed and was stirred for 16 h. The volatiles were removed under vacuum, pentane (50 mL) was added to the residue and the mixture was filtered. After the filtrate was concentrated to 10 mL and stored at −20°C for a week, a colorless crystalline solid was isolated (0.95 g, 21% yield based on Zn). The compound decomposed at 194°C without melting. IR (KBr pellet): ν_{N-H}, 3404 (shoulder), 3384, 3332, 3310, 3269, 3178 cm^{-1}. Anal. Calcd for $C_{56}H_{91}N_5Zn_2$ (%): C, 69.69; H, 9.50; N, 7.26. Found (%): C, 70.22; H, 9.86; N, 7.11. The existence of four unique amido ligands (based on the solid-state structure) complicated the ^{1}H NMR spectrum. Identifiable resonances assignable to HN^{i}Bu$_2$ ligand appeared at δ 0.74 (d, CH_3), 1.55 (m, CH), and 2.28 (overlapping doublets, CH_2). Multiple, overlapping resonances from the ^{i}Pr$_2$C$_6$H$_3$ groups were located at δ 0.8–1.2 (CH_3), 2.2–3.6 (CH), and 6.8–7.0 (aromatic). Two broad singlets at 0.33 and 4.25 were assigned to NH resonances. Integration confirmed the presence of one HN^{i}Bu$_2$ ligand per four ^{i}Pr$_2$C$_6$H$_3$ groups. In the ^{13}C NMR spectrum, HN^{i}Bu$_2$ resonances were found at δ 20.9 (CH_3), 28.4 and 28.8 (CH), and 58.2 (CH_2). Broad ^{i}Pr$_2$C$_6$H$_3$ resonances were found at δ 22.9 and 24.2 for CH_3, 28.7 for CH, and 123.3–134.5 for the aromatic carbons.

2.4. *Single crystal XRD data collection, structure solution, and refinement*

A Bruker SMART Platform CCD diffractometer was used for data collection. A crystal (dimensions $0.30 \times 0.15 \times 0.10$ mm^3) was placed on a glass capillary under N_2 and mounted on the diffractometer. The data were collected at 173(2) K using Mo-Kα radiation (graphite monochromator) with a frame time of 45 s and a detector distance of 4.965 cm. A preliminary set of cell constants was calculated from reflections harvested from three sets of 20 frames. These initial sets of frames were oriented such that orthogonal wedges of reciprocal space were surveyed. This produced initial orientation matrices determined from 85 reflections. For the data collection, a randomly oriented region of reciprocal space was surveyed to the extent of one sphere and to a resolution of 0.84 Å. Three major sections of frames were collected with 0.30° steps in ω at three different φ settings and a detector position of −28° in 2θ. The intensity data were corrected for absorption and decay (SADABS). Final cell constants were calculated from the xyz centroids of 4021 strong reflections from the actual data collection after integration (SAINT). The experimental conditions and unit cell information are summarized in table 1. The structure was solved using SIR97 and refined using SHELXL-97. The space group $P2_1/n$ was determined based on systematic absences and intensity statistics. A direct-methods solution was calculated which provided most non-hydrogen atoms from the E-map. Full-matrix least-squares/difference Fourier cycles were performed which located the remaining non-hydrogen atoms. All non-hydrogen atoms were refined with anisotropic displacement parameters. All hydrogens on nitrogen were placed from the difference map and refined with relative isotropic displacement parameters. All remaining hydrogens were placed in ideal positions and refined as riding atoms with relative isotropic displacement parameters. The final full-matrix least-squares refinement converged to $R_1 = 0.0372$ and

Table 1. Crystallographic data for [Zn(NH-2,6-^{i}Pr$_2$C$_6$H$_3$)$_2$]$_2$(HN^{t}Bu$_2$).

Empirical formula	$C_{56}H_{91}N_5Zn_2$
Formula weight	965.08
Color, morphology	Colorless, block
Crystal size (mm^3)	$0.30 \times 0.15 \times 0.10$
Crystal system	Monoclinic
Space group	$P2_1/n$
Unit cell dimensions (Å, °)	
a	15.7065(12)
b	20.5332(15)
c	17.3306(13)
β	92.0210(10)
Volume (Å^3), Z	5585.7(7), 4
Temperature (°C)	−100
Wavelength (Å)	0.71073
Total reflections	40,866
Independent reflections	9868, R(int) = 0.0436
Observed reflections	7272
Completeness to $\theta = 25.04$ (%)	99.9
Absorption correction	Multi-scan
R_1 [$I > 2\sigma(I)$], wR_2 (all data)[a]	0.0372, 0.0974

[a] $R_1 = \sum||F_o| - |F_c||/\sum|F_o|$ and $wR_2 = \{\sum[w(F_o^2 - F_c^2)^2]/\sum[w(F_o^2)^2]\}^{1/2}$, where $w = q/[\sigma^2(F_o^2) + (aP)^2 + bP + d + e\sin(\theta)]$, $P = (F_o^2 + 2F_c^2)/3$.

$wR_2 = 0.0974$ (F^2, all data). One of the isopropyl groups, C(42)–C(44), was modeled as being disordered over two positions (68 : 32).

3. Results

3.1. *Reaction overview*

The general synthetic procedure is reported elsewhere [5] and is outlined in scheme 1. Two stages are involved corresponding to the separate addition of reactants. In stage 1, the reaction of [Zn(N^{t}Bu$_2$)$_2$]$_2$ with two equivalents of hexylamine for 18 h at room temperature in a nitrogen atmosphere afford a clear solution. Stage 2 involved the exposure of this solution to a flow or air maintained at a constant relative humidity ranging from 19% to 68% for a period of 2.5–4 days. The atmosphere provides both H_2O and CO_2, and the diameter of nanocrystals increases in size as the relative humidity increases. The CO_2 is incorporated into the product as hexylammonium hexylcarbamate (HAHC). At the end of stage 2 a yellow, waxy residue remains. After a multi-step purification, 3.7–5.3 nm white, free-flowing ZnO nanocrystals capped with hexylammonium hexylcarbamate are obtained in 75%–85% yield (on a Zn basis).

3.2. *Stage 1*

In the first stage of the ZnO nanocrystal synthesis, [Zn(N^{t}Bu$_2$)$_2$]$_2$ is made to react with two equivalents of hexylamine in Et_2O under N_2. A white insoluble material forms

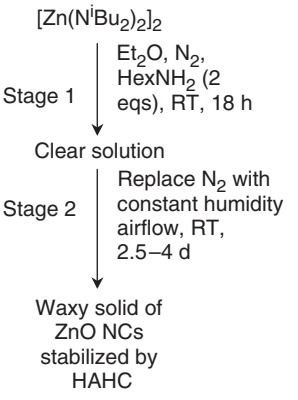

Scheme 1.

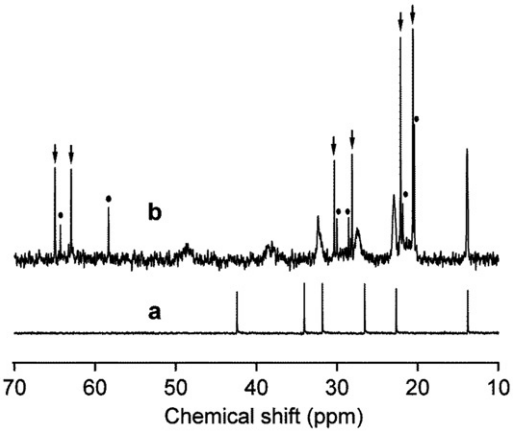

Figure 1. ^{13}C NMR spectra of (a) hexylamine and (b) compounds isolated from the reaction of $[Zn(N^iBu_2)_2]_2$ with two equivalents of hexylamine. The arrows mark the resonances that were assigned to $[Zn(N^iBu_2)_2]_2$. The dots mark the resonances of the second type of N^iBu_2.

immediately after the two reactants are mixed, which dissolves after a few hours and the reaction is stirred for a total of 18 h to afford a clear solution. After the reaction, the solvent and volatile products are removed to isolate a colorless, viscous liquid. The ^{13}C NMR spectrum (b) of this material is shown in figure 1, along with the comparison to the hexylamine (a). The resonances at 21.4, 23.0, 28.9, 31.1, 63.6, and 65.6 ppm (marked with arrows) in (b) are assigned to $[Zn(N^iBu_2)_2]_2$ by comparing with the pure compound. The resonances at 21.3, 22.7, 28.9, 30.8, 59.0, and 64.9 ppm (marked with dots) are clearly identifiable as belonging to different, uncharacterized N^iBu_2-containing compound(s). The remaining six broader peaks at 14.7, 23.8, 28.2, 33.1, 38.8, and 49.5 ppm are attributed to the hexylamido ligand, perhaps in $[Zn(NHhex)_2]_n$. It should be noted that because of the different degree of peak broadening, the N^iBu_2 and hexylamido ligands may belong to different compounds in

the solution. Consistent with the ^{13}C NMR results, the ^{1}H NMR spectrum of the mixture consists of broad hexylamido resonances and sharp $N^{i}Bu_2$ resonances.

3.3. *Stage 2*

Room temperature nanocrystal growth is monitored in a synthesis with a humidity of $35 \pm 1\%$. After the Et_2O solution, which is formed from the reaction of $[Zn(N^{i}Bu_2)_2]_2$ and hexylamine, is exposed to moist air, a white precipitate appears within a day. This solid disappears as the reaction proceeded to 83 h, which indicates the starting point of the formation of *dispersible* ZnO NCs. From this time on, seven ZnO NCs samples are obtained by isolating aliquots of the solution at different times followed by filtration and removal of volatiles. The XRD results of the ZnO NC samples are shown in figure 2, and the XRD size *versus* reaction time is plotted in the inset. The diffraction patterns compare well with that reported for ZnO in JCPDS card 36-1451. The NCs isolated at 83 h exhibit a size of 2.8 nm. These grow to 3.7 nm by 113 h at which point further growth ceases. At 113 h the volume of the solution is *ca* 2 mL, which means that the crystal growth had ceased even though there was still a liquid phase remaining.

The volatile products are collected in a liquid N_2 trap from the solution isolated at 95–119 h. ^{1}H NMR and ^{13}C NMR spectra of all of these samples are similar. ^{1}H NMR spectra establish that the major species of the trapped volatiles is $HN^{i}Bu_2$. The minor components are more clearly identified in the ^{13}C NMR spectrum. In addition to strong 58.1, 28.0, and 20.4 ppm resonances attributed to $HN^{i}Bu_2$, two sets of resonances related to hexylamine are present. One set of resonances at 42.1, 33.8, 31.4, 26.3, 22.3, and 13.7 ppm are very close to those of pure hexylamine and the other set consists of seven peaks at 170.0, 61.2, 33.6, 31.5, 30.5, 26.6, and 19.1 ppm. Comparing to the ^{13}C NMR data in the literature for carbamates and alkylammonium ions [5], we propose that the two sets of resonances result from a hexylammonium hexylcarbamate, $[NH_3(CH_2)_5CH_3]^{+}[CH_3(CH_2)_5N(H)C(O)O]^{-}$. It should be pointed out that while the 170.0 and 61.2 ppm peaks are uniquely attributed to the carbamate ion, the assignments of other resonances are tentative because of the similarity in the chemical shifts for the two types of hexyl carbons not directly bonded to the functional groups.

3.4. *Synthesis and characterization of $[Zn(NH\text{-}2,6\text{-}^{i}Pr_2C_6H_3)_2]_2(HN^{i}Bu_2)$*

The reaction of the bulky amine, 2,6-$^{i}Pr_2C_6H_3NH_2$, with $[Zn(N^{i}Bu_2)_2]_2$ allows isolation of $[Zn(NH\text{-}2,6\text{-}^{i}Pr_2C_6H_3)_2]_2(HN^{i}Bu_2)$ in 21% yield (based on Zn). Elemental analysis is in good agreement with the formula. IR spectroscopy exhibits ν_{N-H} absorptions at 3404, 3384, 3332, 3310, 3269, and 3178 cm^{-1}. The ^{1}H and ^{13}C NMR spectra exhibit broad resonances. These IR and NMR features are consistent with the findings from the single-crystal X-ray analysis (figure 3), where all four arylamido ligands were unique.

$[Zn(NH\text{-}2,6\text{-}^{i}Pr_2C_6H_3)_2]_2(HN^{i}Bu_2)$ crystallizes in space group $P2_1/n$ with one molecule in the asymmetric unit. Selected bond lengths and angles are given in table 2. The structure exhibits a slightly folded Zn_2N_2 ring formed from Zn and arylamido nitrogens, as seen by the torsion angle of N(3)–Zn(2)–N(4)–Zn(1) (2.13(10)°). Each Zn is also bonded to a terminal arylamido ligand and $HN^{i}Bu_2$ is attached to Zn(1). Both three- and four-coordinate Zn's are present in the molecule. The geometry around Zn(1)

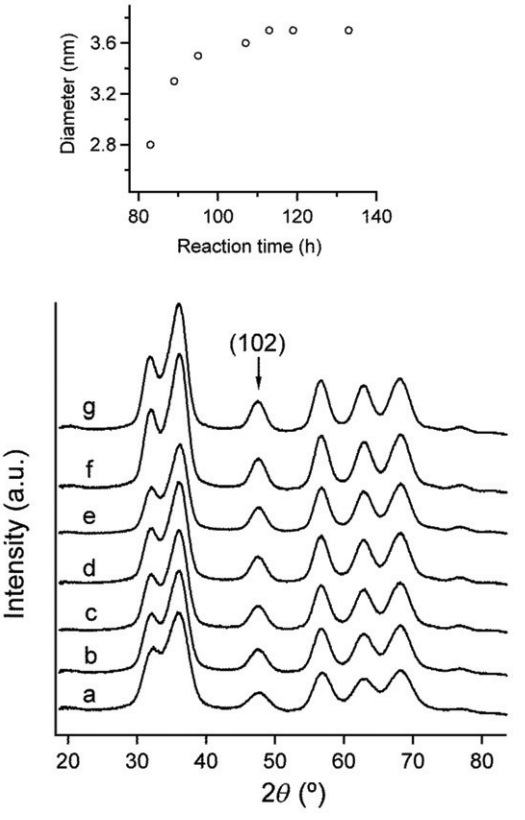

Figure 2. XRD patterns of the ZnO nanocrystals isolated from the synthesis using $35 \pm 1\%$ humidity at different times of (a) 83 h, 2.8 nm, (b) 89 h, 3.3 nm, (c) 95 h, 3.5 nm, (d) 107 h, 3.6 nm, (e) 113 h, 3.7 nm, (f) 119 h, 3.7 nm, and (g) 133 h, 3.7 nm. The inset shows the plot of nanocrystal sizes *vs.* reaction time.

is approximately tetrahedral. Zn(2) is three-coordinate with trigonal planar geometry (the sum of the three N–Zn(2)–N angles is 359.9(3)°). The nitrogens of the terminal arylamido ligands are trigonal planar.

The structure of the Zn_2N_2 ring exhibits distortions consistent with the presence of the three and four coordination numbers of Zn(2) and Zn(1), respectively. The N(3)–Zn(2)–N(4) bond angle (92.33(9)°) is typical for three-coordinate zinc diamides, as found to be 91.06(8)–93.37(9)° in $\{Zn[N(SiMe_2CH_2)_2]_2\}_2$ [7], $\{Zn[N(SiMe_3)Ph]_2\}_2$ [8], $[Zn(NPh_2)_2]_2$ [9], $\{Zn[N(CH_2Ph)_2]_2\}_2$ [10], and $[Zn(N^tBu_2)_2]_2$ [6]. The bond angle on the four-coordinate Zn, N(3)–Zn(1)–N(4) (85.94(9)°) is comparable to those in $[ZnEt(NHmesityl)(THF)]_2$ (85.8(2)° and 86.5(2)°) [11], but smaller than those in $[ZnMe(NHadamantyl)]_2(NH_2adamantyl)(THF)$ (89.40(5)°, 91.47(5)°) [12] and in $\{ZnMe[N(CH_2CH_2NMe_2)_2]\}_2$ (93.23(7)°) [13], $\{Zn[N(CH_2CH_2NMe_2)_2]_2\}_2$ (90.19(8)° and 91.66(8)°) [13] and $\{ZnR[N(Me)(CH_2)_nNMe_2]\}_2$ ($n = 2$ or 3 and R = Me or Et) (89.4(2)–91.22(10)°) [14]. The small N(3)–Zn(1)–N(4) bond angle as well as the unusual Zn–N bond lengths described below are attributed to substantial steric repulsion among the bulky ligands around Zn(1). The bond angles on the ring nitrogens, Zn(1)–N(3)–Zn(2) (90.17(9)°) and Zn(2)–N(4)–Zn(1) (91.49(9)°), are similar to those in compounds

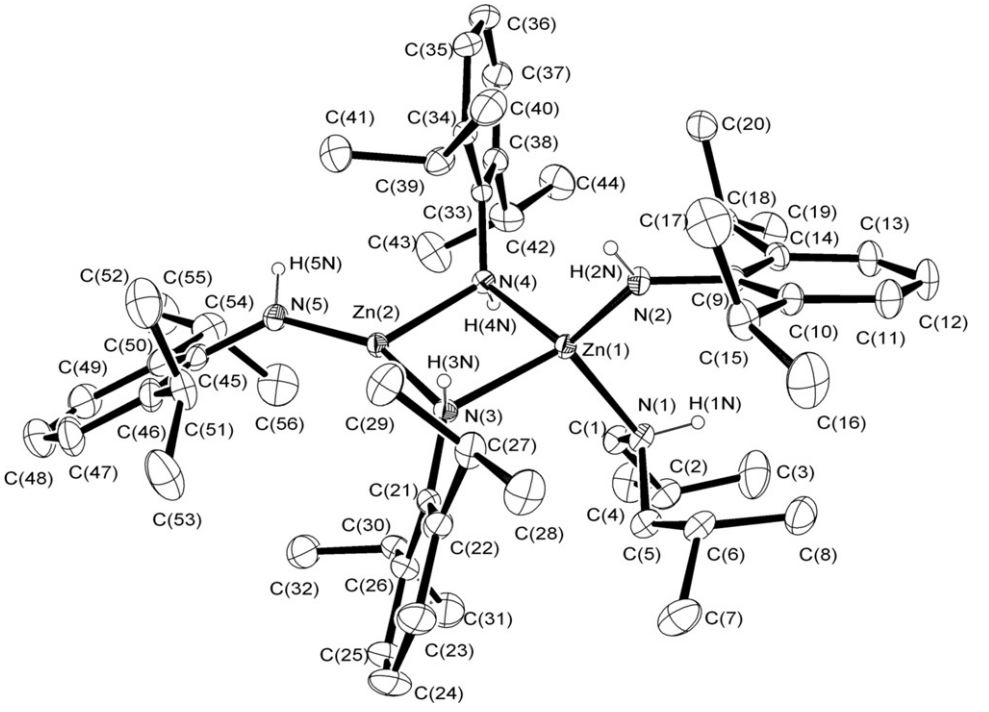

Figure 3. X-ray single-crystal structure of $[(2,6\text{-}^{i}Pr_2C_6H_3NH)_2Zn]_2(HN^{i}Bu_2)$ showing 20% thermal ellipsoids. Hydrogens except those on nitrogen are omitted for clarity.

Table 2. Selected bond lengths (Å) and angles (deg) for $[(2,6\text{-}^{i}Pr_2C_6H_3NH)_2Zn]_2(HN^{i}Bu_2)$.

Zn(1)–N(1)	2.088(2)	Zn(1)–N(2)	1.923(2)	Zn(1)–N(3)	2.170(2)
Zn(1)–N(4)	2.062(2)	Zn(2)–N(3)	1.968(2)	Zn(2)–N(4)	2.033(2)
Zn(2)–N(5)	1.859(2)				
N(1)–Zn(1)–N(2)	109.40(10)	N(1)–Zn(1)–N(3)	109.63(10)	N(1)–Zn(1)–N(4)	113.51(9)
N(2)–Zn(1)–N(3)	115.98(9)	N(2)–Zn(1)–N(4)	120.39(9)	N(3)–Zn(1)–N(4)	85.94(9)
N(3)–Zn(2)–N(4)	92.33(9)	N(3)–Zn(2)–N(5)	150.78(10)	N(4)–Zn(2)–N(5)	116.81(10)
C(1)–N(1)–Zn(1)	111.00(17)	C(1)–N(1)–C(5)	115.6(2)	C(1)–N(1)–H(1N)	112.0(19)
C(5)–N(1)–Zn(1)	112.31(19)	C(5)–N(1)–H(1N)	97.8(19)	Zn(1)–N(1)–H(1N)	107.1(19)
C(9)–N(2)–Zn(1)	125.95(18)	C(9)–N(2)–H(2N)	117.0	Zn(1)–N(2)–H(2N)	117.0
C(21)–N(3)–Zn(1)	131.65(18)	C(21)–N(3)–Zn(2)	127.17(18)	Zn(1)–N(3)–Zn(2)	90.17(9)
Zn(1)–N(3)–H(3N)	91(2)	Zn(2)–N(3)–H(3N)	103(2)	C(21)–N(3)–H(3N)	106(2)
C(33)–N(4)–Zn(1)	125.01(17)	C(33)–N(4)–Zn(2)	120.49(17)	Zn(2)–N(4)–Zn(1)	91.49(9)
Zn(1)–N(4)–H(4N)	103(2)	Zn(2)–N(4)–H(4N)	105(2)	C(33)–N(4)–H(4N)	109(2)
C(45)–N(5)–Zn(2)	134.3(2)	C(45)–N(5)–H(5N)	112.9	Zn(2)–N(5)–H(5N)	112.9

containing bridging primary amido ligands, $[ZnMe(NHadamantyl)]_2(NH_2adamantyl)$-(THF) (89.47(5)° and 89.64(5)°) [12] and $[ZnEt(NHmesityl)(THF)]_2$ (90.4(2)° and 89.5(2)°) [11].

Among the seven Zn–N bonds in $[Zn(NH\text{-}2,6\text{-}^{i}Pr_2C_6H_3)_2]_2(HN^{i}Bu_2)$, the general trend is that the bonds to the three-coordinate Zn are shorter. For the terminal amides, Zn(2)–N(5) (1.859(2) Å) is shorter than Zn(1)–N(2) (1.923(2) Å) and for the bridging

bonds, Zn(2)–N(3) (1.968(2) Å) and Zn(2)–N(4) (2.033(2) Å) are shorter than Zn(1)–N(4) (2.062(2) Å) and Zn(1)–N(3) (2.170(2) Å). The terminal Zn–N bond lengths fall in the range of those reported in the literature, for example, 1.844(2)–1.902(2) Å in the three-coordinate Zn compounds [6–10, 15], and 1.919(4)–1.927(5) Å in the four-coordinate Zn compounds, $Zn(NPh_2)_2(THF)_2$ [9] and $\{Zn[(NMeSiMe_2)_2NMe](pyridine)\}_2$ (1.940(4) Å) [16]. As mentioned, the crowdedness around Zn(1) generates atypical Zn–N bond lengths. The difference between Zn(1)–N(3) and Zn(1)–N(4) bond lengths is large. In addition, the bond of the neutral ligand HN^iBu_2 to Zn, Zn(1)–N(1) (2.088(2) Å) is even shorter than one of the bridging bonds, Zn(1)–N(3), which is contrary to other diamido zinc compounds containing a dative Zn–N bond such as $\{Zn[N(CH_2CH_2NMe_2)_2]_2\}_2$ (2.176(2) Å) [13].

4. Discussion

The transformation of $[Zn(N^iBu_2)_2]_2$ into nanocrystalline zinc oxide occurs in two stages. In the first, hexylamine reacts with the zinc amide to replace the secondary amides with primary amides. Hexylamine is one of the several saturated linear alkylamines used in this reaction. It became the amine of choice because excess hexylamine is sufficiently volatile to be removed from the reaction by evaporation. Reactions conducted with octyl or dodecylamine also produce the desired products, but we were unable to isolate free-flowing powders using dodecylamine or other longer chain amines. Clear dispersions of ZnO are not formed when butyl- and shorter chain amines are used as the surfactant.

4.1. *Stage 1*

Three observations provide some insight into this reaction. First, the stoichiometry is important. A ratio of two hexylamines/zinc ion in the initial complex leads to an intractable solid. Addition of excess hexylamine or diisobutylamine to this solid does not change its intractability. This stoichiometry would be consistent with the reaction shown in equation 1.

$$n[Zn(N^iBu_2)_2]_2 + 4n\ HexNH_2 \rightarrow [Zn(NHhex)_2]_{2n} + 4n\ HN^iBu_2 \quad (1)$$

Second, all $[Zn(N^iBu_2)_2]_2$ and hexylamine are consumed upon addition of a 1 : 1 ratio of hexylamine/zinc. Diisobutylamine is detected as a product in this reaction. This suggests that the rate of substitution of the second diisobutylamido ligand is slower than that of the first and that an intermediate zinc species is formed bearing both hexylamido and diisobutylamido ligands. Third, after approximately 3 h the mixture resulting from the 1 : 1 stoichiometry reaction becomes clear and NMR spectroscopy shows evidence of HN^iBu_2, the *reappearance* of $[Zn(N^iBu_2)_2]_2$ and broad peaks consistent with hexyl groups bound to a soluble, oligomeric species. This mixture will be identified as the "precursor solution".

A possible explanation for the effect of stoichiometry is that the initial precipitate in the 1 : 1 stoichiometry reaction contains a mixture of both hexylamido and

diisobutylamido ligands. With time, ligand redistribution occurs to reform $[Zn(N^iBu_2)_2]_2$ and a soluble, oligomeric (rather than polymeric) form of $[Zn(NHhex)_2]_n$.

The stoichiometric reaction of $[Zn(N^iBu_2)_2]_2$ with four equivalents of 2,6-diisopropylaniline provides strong evidence that all of the diisobutylamido ligands can be replaced. The steric bulk of the anilide ligand prevents polymerization that is expected with smaller amines.

4.2. *Stage 2*

Diisobutylamine, $[Zn(N^iBu_2)_2]_2$ and $[Zn(NHhex)_2]_n$ comprise the clear ether precursor solution at the beginning of Stage 2. During this stage, the zinc–amide bonds are hydrolyzed, CO_2 is absorbed and converted into a carbamate, liquids (ether, diisobutylamine, and hexylamine) evaporate and condensation ultimately leads to the nucleation and growth of zinc oxide nanocrystals. At the end of Stage 2 (i.e., completion of the synthesis) high yields of ZnO NCs capped with hexylammonium hexylcarbamate are isolated as a waxy solid. Stage 2 can be further divided into two parts. The first begins at the point when moist air hits the clear precursor solution to produce a cloudy mixture, and the second begins when the solution again becomes clear. Figure 2 shows the growth of ZnO nanocrystals throughout the second part of stage 2.

There are two important observations associated with figure 2. First, extrapolation of the relatively rapid growth from between 80 and 90 h back to zero particle diameter indicates a long induction period for ZnO formation. Second, the growth eventually stops as the liquid components evaporate. Virtually all of the diethyl ether evaporated by the beginning of the second part of Stage 2 leaving diisobutylamine and hexylamine to serve as the solvent in the last stage of the process.

We have little insight into Stage 2 chemistry. The monodisperse product suggests that nucleation events are isolated at an early point in the reaction. XRD measurements of dried powders extracted during the early stages show broad peaks consistent with ZnO. It is unknown if additional, molecular precursors remain after the initial nucleation of ZnO, to react more slowly with the nuclei thus allowing growth. The alternative would involve a ripening process in which the smaller particles serve as a nutrient source for the growth of larger particles.

The steps outlined in this synthesis are consistent with the observations of Kahn *et al.* [17] for the ZnO NC synthesis based on dicyclohexylzinc. Both methods provide a room temperature approach to monodisperse ZnO nanocrystals.

Acknowledgments

We thank Victor G. Young, Jr and Benjamin Kucera of the University of Minnesota, Department of Chemistry X-ray Laboratory, for the crystal structure. This research was supported in part by grants from the Initiative for Renewable Energy and the Environment at the University of Minnesota and Xcel Energy under their Renewable Development Fund.

References

[1] U. Ozgur, Y.I. Alivov, C. Liu, A. Teke, M.A. Reshchikov, S. Dogan, V. Avrutin, S.J. Cho, H. Morkoc. *J. Appl. Phys.*, **98**, 041301/1 (2005).
[2] U. Koch, A. Fojtik, H. Weller, A. Henglein. *Chem. Phys. Lett.*, **122**, 507 (1985).
[3] E.A. Meulenkamp. *J. Phys. Chem. B*, **102**, 7764 (1998).
[4] L. Spanhel. *J. Sol–Gel Sci. Technol.*, **39**, 7 (2006).
[5] B. Luo, J.E. Rossini, W.L. Gladfelter. *Langmuir*, **25**, 13133 (2009).
[6] H. Schumann, J. Gottfriedsen, F. Girgsdies. *Z. Anorg. Allgem. Chem.*, **623**, 1881 (1997).
[7] O. Just, D.A. Gaul, W.S. Rees. *Polyhedron*, **20**, 815 (2001).
[8] H. Schumann, J. Gottfriedsen, S. Dechert, F. Girgsdies. *Z. Anorg. Allgem. Chem.*, **626**, 747 (2000).
[9] M.A. Putzer, A. Dashti-Mommertz, B. Neumueller, K. Dehnicke. *Z. Anorg. Allgem. Chem.*, **624**, 263 (1998).
[10] D.R. Armstrong, G.C. Forbes, R.E. Mulvey, W. Clegg, D.M. Tooke. *J. Chem. Soc., Dalton Trans.*, 1656 (2002).
[11] M.M. Olmstead, W.J. Grigsby, D.R. Chacon, T. Hascall, P.P. Power. *Inorg. Chim. Acta*, **251**, 273 (1996).
[12] M. Westerhausen, T. Bollwein, A. Pfitzner, T. Nilges, H.-J. Deiseroth. *Inorg. Chim. Acta*, **312**, 239 (2001).
[13] B. Luo, B.E. Kucera, W.L. Gladfelter. *Polyhedron*, **25**, 279 (2006).
[14] M.A. Malik, P. O'Brien, M. Motevalli, A.C. Jones. *Inorg. Chem.*, **36**, 5076 (1997).
[15] S.C. Goel, M.Y. Chiang, W.E. Buhro. *Inorg. Chem.*, **29**, 4646 (1990).
[16] A.J. Elias, H.G. Schmidt, M. Noltemeyer, H.W. Roesky. *Organometallics*, **11**, 462 (1992).
[17] M.L. Kahn, M. Monge, V. Colliere, F. Senocq, A. Maisonnat, B. Chaudret. *Adv. Func. Mater.*, **15**, 458 (2005).